GEODESIC-BASED PAVEMENT SHADOW REMOVAL REVISITED

Qin Zou[1,2] *Zhongwen Hu*[3] *Long Chen*[4] *Qian Wang*[1,2] *Qingquan Li* [*,3]

[1]State Key Laboratory of Software Engineering, Wuhan University, P.R. China
[2]School of Computer Science, Wuhan University, P.R. China
[3]Shenzhen Key Laboratory of Spatial Smart Sensing and Service, Shenzhen University, P.R. China
[4]School of Mobile Information Engineering, Sun Yat-Sen University, P.R. China
qzou@whu.edu.cn, zwhoo@szu.edu.cn, chenl46@mail.sysu.edu.cn, qianwang@whu.edu.cn, liqq@szu.edu.cn

ABSTRACT

Shadows often incur uneven illumination to pavement images, which brings great challenges to image-based pavement crack detection. Thus, it is desired to remove pavement shadows before detecting pavement cracks. However, due to the large penumbras cast by trees, light poles, etc., it is difficult to locate shadows in a pavement image. In this paper, an automatic pavement shadow removal method is proposed based on geodesic analysis. First, a geodesic shadow model is used to partition a pavement shadow into a number of geodesic regions. Then, an optimal background region is selected for reference by statistic analysis. Finally, a texture-balanced illuminance compensation is applied on all geodesic regions over the image. Experiments demonstrate the effectiveness of the proposed method.

Index Terms— shadow removal, penumbra area, pavement shadow, crack detection, texture balance

1. INTRODUCTION

Modern road maintenance has a strong demand for automatic pavement crack detection. In the past ten years, image-based pavement crack detection and classification has been a research focus in both academia and industry [1, 2, 3]. However, when pavement images are contaminated by shadows, many complications arise and undermine the performance of crack detection methods . This is because, pavement shadows not only destroy the uniform illuminance of pavement images, but also decrease the contrast of pavement cracks in the shadow regions. Thus, a shadow removal procedure is commonly required before detecting the pavement cracks.

In the past two decades, a number of algorithms have been developed to remove shadow from images [4, 5, 6, 7, 8, 9, 10]. Typically, there are two key steps in shadow removal. One is shadow-region location, and the other is illuminance compensation. To locate the shadow regions, interactive methods [11, 12, 13, 14, 15, 16] and automatic methods [17, 18, 19, 20, 21] have been studied. In [11], an image was interactively partitioned into the shadow region, non-shadow region and penumbra, which were fed into a Bayesian network as priori probability, to seek an optimal compensation in illuminance. In [12], a point was set in advance in the shadow region and the whole shadow region was obtained through seed growing. In [14], a shadow stroke was developed to select the penumbra area with human interaction, similar work was found in [15]. In [16], interactive graph cut was utilized to segment the shadow regions from background. While interactive methods often fall short in efficiency, machine-learning based automatic methods have been exploited in [19, 17].

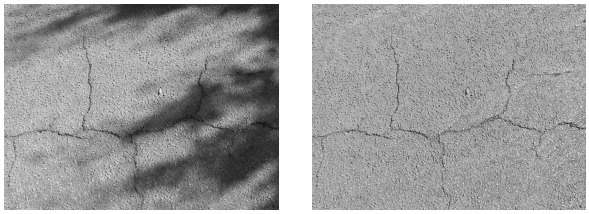

(a) (b)

Fig. 1. An example of pavement shadow removal with the proposed method. (a) A pavement image, (b) the result.

Pavement shadows are difficult to handle owing to the existence of large penumbra areas, as shown in Fig. 1(a). A number of methods have been studied to handle the penumbra. In [22], the gradient of the shadow boundary was set to zero, interactively. After shadow removal, a 2D Poisson algorithm [23] was applied to recover the shadow boundary. This method assumes a recognizable shadow boundary, which would lose texture information of the penumbra. To alleviate this problem, image inpainting techniques were employed in [12] to restore the texture in penumbra. However, the resulting textures cannot avoid to bias from the original. In [24], the intensity distribution of the shadow was supposed to be a

This research is supported by the National Natural Science Foundation of China (NSFC) under grant No. 61301277 and No. 41371431, the National Basic Research Program of China (973 Program) under grant No. 2012CB725303, and the Hubei Provincial Natural Science Foundation under grant No. 2013CFB299. *Corresponding author: Dr. Q.Q. Li.

curved surface, and the texture in the penumbra area was restored by illuminance compensation which flattens the curved surface. Similar method was presented in [14]. However, these two methods require interactions to locate the penumbra area, which heavily limits their applications in practice.

In this study, we partition the large penumbra of pavement shadow with a geodesic shadow model. Then, we select an optimal reference areas for illuminance compensation by analyzing statistic property of the geodesic regions. In illuminance compensation, textures and intensities are both balanced. Moreover, the proposed method processes every geodesic region, which guarantees an even illuminance over the whole image.

In the rest of this paper, Section 2 introduces our prior work on geodesic shadow removal. Section 3 describes the proposed shadow removal method. Section 4 reports experimental results and Section 5 concludes the paper.

2. GEODESIC SHADOW REMOVAL

The geodesic shadow removal (GSR) algorithm was proposed in our prior work [25]. In broad engineering practices, GSR has mostly expressed a great power in handling pavement shadows. However, it also shows weaknesses in some cases. In this section, we first briefly overview GSR, and then examine its weaknesses.

2.1. Geodesic Shadow Removal Algorithm

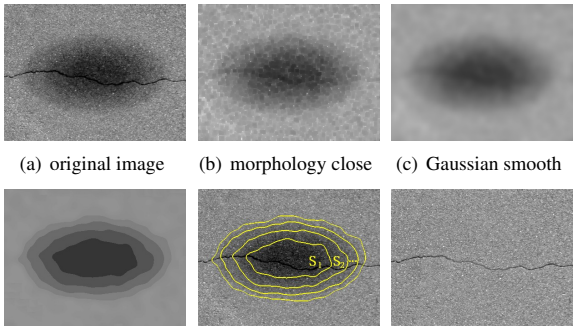

(a) original image (b) morphology close (c) Gaussian smooth

(d) geodesic leveling (e) shadow regions (f) illum. compensate.

Fig. 2. An illustration to GSR.

GSR consists of four main steps, as illustrated in Fig. 2. In the following, we introduce each step of them.

i) *Morphology close*. Note that, cracks often have similar intensities with shadows, and a morphological close removes the cracks. As a result, in shadow-area estimation, the cracks will not be counted into the shadows. In Fig. 2, (a) is a pavement image, and (b) shows the result.

ii) *Gaussian smooth*. As pavement is featured with strong grain-like textures, a Gaussian smooth operation will make shadow-area estimation not be influenced by the textures. Figure 2(c) shows the smoothed result.

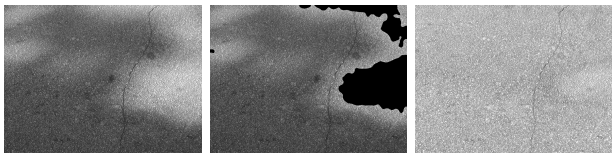

(a) (b) (c)

Fig. 3. An example to illustrate the weakness of GSR. (a) An original pavement image. (b) The reference area (in black) extracted by GSR. (c) Shadow-removal result by GSR.

iii) *Geodesic leveling*. By using a watersheding strategy, the whole smoothed image is partitioned into a series of geodesic regions in ascending average illuminance, i.e., $\{G_i|i = 1, ..., L, ..., N\}$. Suppose S and B be the shadow area and background (non-shadow area), then $S = \{G_i|i = 1, 2, \ldots, L\}$, and $B = \{G_i|i = L{+}1, L{+}2, \ldots, N\}$. In GSR, L is empirically set as $L = \frac{7}{8}N$. Example results are shown in Fig. 2(d) and (e).

iv) *Illuminance compensation*. After we get the shadow from the geodesic levels, i.e., S_i(=G_i), an illuminance compensation operation is applied to each shadow level. Given $I_{i,j}$ be the intensity of the pixel at (i, j), and $I'_{i,j}$ be the illuminance-compensation result, S and B be the shadow region and the background (non-shadow region), then each pixel $(i, j) \in S$ is assigned with a new value $I'_{i,j} = \alpha \cdot I_{i,j} + \lambda$. Here $\alpha = \frac{D_B}{D_S}$, and $\lambda = \hat{I}_B - \alpha \cdot \hat{I}_S$. Note that, D_S and D_B are the standard deviations of the intensity in S and B, respectively, $\hat{I}_S$ and $\hat{I}_B$ are the average intensities. Figure 2(f) shows the illuminance-compensation result.

2.2. Weaknesses of GSR

The strong points of GSR lie in that, first, it locates the shadow regions using a geodesic leveling strategy which well handles the large penumbra area of pavement shadows. Second, in step iv, by introducing a multiplicative factor α to illuminance compensation, it can increase the contrast of the shadow regions to the level of the background region, which leads to a texture-balanced compensation result. Third, it utilizes a morphological close step to remove cracks and keep cracks out from geodesic leveling, which preserves cracks in the shadow-removal results.

One weak point of GSR is found in the selection of the shadow regions S and the background B in the step iii. To be specific, first, it is not reliable to separate the shadow and the non-shadow area by consistently setting L=$\frac{7}{8}N$. Second, it does not always work to take the whole background area, i.e., the intensity levels from $\frac{7}{8}N$ to N, as the reference area for illuminance compensation, especially when there's over-illuminance in the identified B. An example is shown in

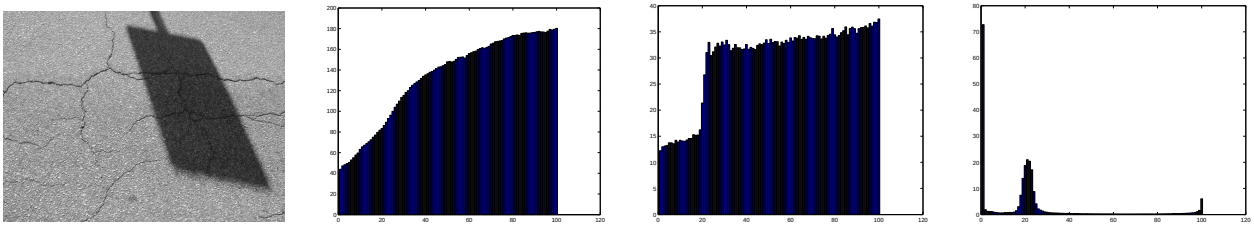

(a) (b) (c) (d)

Fig. 4. Statistic values on different geodesic levels. (a) A pavement image. (b) Average intensity values ($\mathcal{A}$). (c) Standard deviation values ($\mathcal{D}$). (d) Intensity span values ($\mathcal{H}$). Note that, the indices of the geodesic levels are displayed on the X axis.

Fig. 3. It can be seen from Fig. 3(b) that, the background identified by GSR has been suffered from overexposure. It is improper to take its average intensity and the standard deviation as the reference for illuminance compensation. Figure 3(c) show the final shadow removal result produced by GSR, which is apparently visually unsatisfactory. Moreover, the illuminance in the reference area has been left uneven.

3. IMPROVED GEODESIC SHADOW REMOVAL

We propose to improve GSR on two points. One is to select an optimal reference area for illuminance compensation, the other is to apply illuminance compensation to the whole image. In this section, we introduce this improved GSR (IGSR).

3.1. Optimal Reference Area Seclection

Once the $geoLevel$ operation is applied, a number of geodesic levels can be gained. With these geodesic levels, we can get some statistic information as follows,

$$\mathcal{A}_i = \mathsf{AVE}(G_i),\ \mathcal{D}_i = \mathsf{DEV}(G_i),\ \mathcal{H}_i = \mathsf{SPAN}(G_i),$$

where $\mathsf{AVE}()$ and $\mathsf{DEV}()$ calculate the average intensity and the standard deviation of pixels in one geodesic level, and $\mathsf{SPAN}()$ calculates the span of intensity values in one geodesic level, i.e., (max-min) value. An example is shown in Fig. 4. We find that, geodesic levels corresponding to penumbra area generally have larger $\mathcal{H}$ values than non-shadow regions. Therefore, we roughly estimate the shadow area and the non-shadow area by applying a bi-partitioning algorithm OTSU on the $\mathcal{H}$ values,

$$\{\mathcal{H}^S, \mathcal{H}^B\} = \mathsf{OTSU}(\{\mathcal{H}_i | i = 1, 2, ..., N\}) \qquad (1)$$

where $\mathcal{H}^S$ is one class with lower $\mathcal{H}$ values, which corresponds to the shadow area, and $\mathcal{H}^B$ is the other class corresponds to the non-shadow area. It is desired to produce a shadow-free image with higher intensity and stronger texture, thus we select an optimal reference area using Eq. 2,

$$G_o = arg \max_{G_i} \{(\mathcal{A}_i * \mathcal{D}_i) | \mathcal{H}_i \in \mathcal{H}^B\}. \qquad (2)$$

3.2. Full-level Illuminance Compensation

With an optimal reference area, illuminance compensation can be conducted on all geodesic levels. Specifically, the proposed IGSR can be summarized in the following steps.

- First, a morphological close is applied to the original image, to keep cracks out from shadow-area evaluation.
- Second, a low-pass Gaussian filter with a radius of 25 pixels is used to smooth off the grain-like textures.
- Third, a geodesic leveling is conducted to partition the smoothed image into a number of geodesic regions. This is achieved by a watersheding strategy, where the minimum number of pixels in each geodesic region is n_g.
- Fourth, an optimal reference area is selected from the generated geodesic regions by using Eq. 2.
- Finally, a texture-balanced illuminance compensation, as introduced in section 2.1, is performed on every geodesic region.

Note that, IGSR performs illuminance compensate not only on shadow area but also on non-shadow area. In this way, it can reduce the illuminance of areas suffering from overexposure to the level of the reference area.

4. EXPERIMENTS AND RESULTS

In this section, first, experiments are conducted to validate the proposed IGSR, then the IGSR is compared with GSR, and finally the impact of parameter n_g on IGSR is examined.

4.1. Effectiveness of IGSR

We test the performance of IGSR by a section-intensity analysis. Figure 5 (a) displays an original pavement image with two section lines `Sec. 1` and `Sec. 2`, in which `Sec. 1` crosses the shadow area. Figure 5 (b-d) are shadow-removal results by IGSR in three different settings. It can be seen from Fig. 5 that, all the three results have even illuminance. However, in Fig. 5 (f), the fluctuation of intensity in the shadow area is smaller than that in the non-shadow area, which simply demonstrates a lower contrast in the shadow area than in the non-shadow area. It is because that, illuminance compensation without texture balancing cannot change the contrast in

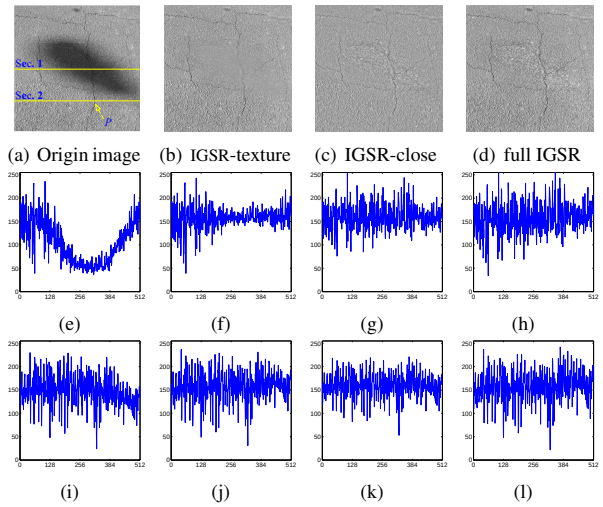

Fig. 5. Comparison of IGSR results under three different settings. (a) A pavement image with two section lines, i.e., `Sec`.1 and `Sec`.2. (b) IGSR-texture: IGSR without texture balancing. (c) IGSR-close: IGSR without morphology close to preserve the cracks. (d) full IGSR. (e)-(h) show the intensity on `Sec`.1 in (a) - (d), respectively. (i)-(l) show the intensity on `Sec`.2 in (a) - (d), respectively.

shadow areas. While in Fig. 5 (g) and (h), similar severity of fluctuation can be found over the whole section, which simply indicates that, the texture-balance illuminance compensation has enhanced the texture of the shadow area. Note that, `Sec`. 2 locates in the non-shadow area, crossing a crack point P. It can be seen from Fig. 5 (i-l) that, the intensity values of P in (i), (j) and (l) stand nearly the same, exactly 23, 25, and 22, which are much lower than that in (k) - a value of 52. It indicates that, without a morphological close, the cracks will be counted into the shadow area, who will then be added with a high intensity value in illuminance compensation. Consequently, the contrast of cracks will be reduced in shadow removal. In summary, the proposed IGSR, i.e., full IGSR, can gain a balanced texture while removing the pavement shadows, and the manipulative factor α is useful to achieve a texture-balanced illuminance compensation, and the morphology close is a necessary step to preserve the cracks.

4.2. IGSR v.s. GSR

Comparisons between IGSR and GSR have been made on a set of pavement images. Two sample images are shown in the left column of Fig. 6, which are suffered from overexposure. It can be seen from Fig. 6 that, shadow-removal results from GSR show an over-bright illuminance, where the illuminance is uneven. However, the results from IGSR hold even-illuminance over the whole image. It is because that, an optimal reference area has been selected by IGSR for illuminance compensation, and the compensation has been performed on all the geodesic levels in the image.

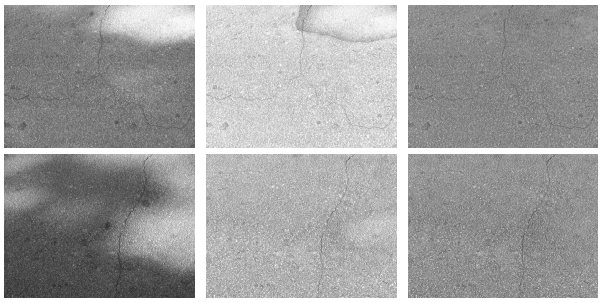

Fig. 6. Comparison of GSR and IGSR. Column 1: two original images. Column 2: GSR results. Column 3: IGSR results.

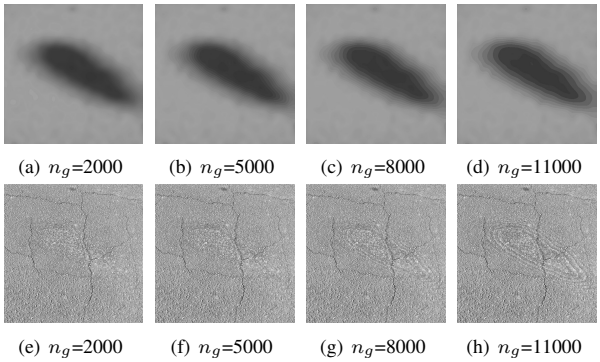

Fig. 7. The impact of n_g on the geodesic leveling and shadow removal. Row 1: geodesic leveling results. Row 2: the corresponding shadow-removal results.

4.3. Impact of parameter n_g

Experiments are also conducted to analyze the impact of n_g on the IGSR result. An illustrative example is shown in Fig. 7, where n_g is tuned from 2000 to 11000, at an interval of 3000. It can be seen from Fig. 7 that, when n_g is tuned from 5000, 8000 to 11000, the intensity jumps between neighboring geodesic regions are increasingly obvious. This is because the geodesic leveling with a larger n_g will partition a wider penumbra annulus into one geodesic region. As the intensity in the penumbra often changes quickly from the shadow center to the background, the average intensity of one geodesic region will significantly bias from that of its neighboring regions. As a result, the illuminance compensation will bring a intensity jump between two neighboring geodesic regions.

5. CONCLUSION

In this work, an improved geodesic-based shadow removal method (IGSR) was proposed to remove pavement shadows. IGRS selected an optimal reference area by analyzing the statistic property of geodesic levels and performed illuminance compensation over all geodesic levels. Experiments demonstrated the superior of IGSR over GSR in handling pavement images suffering from overexposure.

6. REFERENCES

[1] L. Ying and E. Salari, "Beamlet transform-based technique for pavement crack detection and classification," *Computer-Aided Civil and Infrastructure Engineering*, vol. 25, pp. 572–580, 2010.

[2] Q. Li, Q. Zou, D. Zhang, and Q. Mao, "FoSA: F* seed-growing approach for crack-line detection from pavement images," *Image and Vision Computing*, vol. 29, no. 12, pp. 861–872, 2011.

[3] H. Oliveira and P.L. Correia, "CrackIT - an image processing toolbox for crack detection and characterization," in *IEEE ICIP*, 2014, pp. 798–802.

[4] I. Sato, Y. Sato, and K. Ikeuchi, "Illumination distribution from brightness in shadows: adaptive estimation of illumination distribution with unknown reflectance properties in shadow regions," in *ICCV*, 1999.

[5] Y. Weiss, "Deriving intrinsic images from image sequences," in *Proc. of the International Conference on Computer Vision (ICCV'01)*, 2001, pp. 1–8.

[6] J.J. Yoon, C. Koch, and T.J. Ellis, "Shadowflash: an approach for shadow removal in an active illumination environment," in *Proc. of the British Machine Vision Conference (BMVC'02)*, 2002, pp. 1–10.

[7] M.F. Tappen, W.T. Freeman, and E.H. Adelson, "Recovering intrinsic images from a single image," in *Proc. of the Neural Information Processing Systems Conference (NIPS'02)*, 2002, pp. 1–8.

[8] N. Almoussa, "Variational retinex and shadow removal," in *UCLA Technical Report*, 2006.

[9] L. Xu, F.H. Qi, R.J. Jiang, Y.F. Hao, and G.R. Wu, "Shadow detection and removal in real images: A survey," in *SJTU-CVLAB Technical Report*, 2006.

[10] G.D. Finlayson, M. Drew, and C. Lu, "Entropy minimization for shadow removal," *International Journal of Computer Vision*, vol. 85, pp. 35–57, 2009.

[11] T.P. Wu and C.K. Tang, "A bayesian approach for shadow extraction from a single image," in *Proc. of the International Conference on Computer Vision (ICCV'05)*, 2005, pp. 480–487.

[12] Y. Shor and D. Lischinski, "The shadow meets the mask: pyramid-based shadow removal," *Computer Graphics Forum*, vol. 27, no. 2, pp. 577–586, 2008.

[13] A. Mohan, J. Tumblin, and P. Choudhury, "Editing soft shadows in a digital photograph," *IEEE Computer Graphics and Applications*, vol. 27, no. 2, pp. 23–31, 2007.

[14] F. Liu and M. Gleicher, "Texture-consistent shadow removal," in *Proc. of the 10th European Conference on Computer Vision (ECCV'08)*, 2008, pp. 437–450.

[15] Y.F. Su and H.H. Chen, "A three-stage approach to shadow field estimation from partial boundary information," *IEEE Transactions on Image Processing*, vol. 19, no. 10, pp. 2749–2760, 2010.

[16] D. Miyazaki, Y. Matsushita, and K. Ikeuchi, "Interactive shadow removal from a single image using hierarchical graph cut," in *Proc. of the Asian Conference on Computer Vision (ACCV'09)*, 2009, pp. 234–245.

[17] J.J Zhu, K.G.G. Samuel, S.Z. Masood, and M.F. Tappen, "Learning to recognize shadows in monochromatic natural images," in *Proc. of the IEEE Conference on Computer Vision and Pattern Recognition (CVPR'10)*, 2010, pp. 223–230.

[18] E. Salvador, A. Cavallaro, and T. Ebrahimi, "Cast shadow segmentation using invariant color features," *Computer Vision and Image Understanding*, vol. 95, no. 2, pp. 238–259, 2004.

[19] X. Gu, D. Yu, and L. Zhang, "Image shadow removal using pulse coupled neural network," *IEEE Transactions on Neural Networks*, vol. 16, no. 3, pp. 692–698, 2005.

[20] J. Yao and Z. Zhang, "Hierarchical shadow detection for color aerial images," *Computer Vision and Image Understanding*, vol. 102, pp. 60–69, 2006.

[21] S. Audet and J.R. Cooperstock, "Shadow removal in front projection environments using object tracking," in *Proc. of the IEEE CVPR Workshop*, 2007, pp. 1–8.

[22] G.D. Finlayson, S.D. Hordley, and M.S. Drew, "Removing shadows from images," in *Proc. of the 7th European Conference on Computer Vision (ECCV'02)*, 2002, pp. 823–836.

[23] P. Pérez, M. Gangnet, and A. Blake, "Poisson image editing," *ACM Transactions on Graphics*, vol. 22, no. 3, pp. 313–318, 2003.

[24] E. Arbel and H. Hel-Or, "Texture-preserving shadow removal in color images containing curved surfaces," in *Proc. of the IEEE Conference on Computer Vision and Pattern Recognition (CVPR'07)*, 2007, pp. 1–8.

[25] Q. Zou, Y. Cao, Q. Li, Q. Mao, and S. Wang, "CrackTree: Automatic crack detection from pavement images," *Pattern Recognition Letters*, vol. 33, no. 3, pp. 227–238, 2012.